Broadband on-chip polarization mode splitters in lithium niobate integrated adiabatic couplers

HUNG-PIN CHUNG,[1] CHIEH-HSUN LEE,[1] KUANG-HSU HUANG,[1] SUNG-LIN YANG,[1] KAI WANG,[2] ALEXANDER S. SOLNTSEV,[2,3] ANDREY A. SUKHORUKOV,[2] FRANK SETZPFANDT,[4] AND YEN-HUNG CHEN[1,5,*]

[1]*Department of Optics and Photonics, National Central University, Jhongli 320, Taiwan*
[2]*Nonlinear Physics Centre, Research School of Physics and Engineering, The Australian National University, Canberra, ACT 2601, Australia*

[3]*School of Mathematical and Physical Sciences, University of Technology Sydney, Ultimo, NSW 2007, Australia*

[4]*Institute of Applied Physics, Abbe Center of Photonics, Friedrich-Schiller-Universität Jena, 07745 Jena, Germany*

[5]*Center for Astronautical Physics and Engineering, National Central University, Jhongli 320, Taiwan*
**yhchen@dop.ncu.edu.tw*

Abstract: We report, to the best of our knowledge, the first broadband polarization mode splitter (PMS) based on the adiabatic light passage mechanism in the lithium niobate ($LiNbO_3$) waveguide platform. A broad bandwidth of ~140 nm spanning telecom S, C, and L bands at polarization-extinction ratios (PER) of >20 dB and >18 dB for the TE and TM polarization modes, respectively, is found in a five-waveguide adiabatic coupler scheme whose structure is optimized by an adiabaticity engineering process in titanium-diffused $LiNbO_3$ waveguides. When the five-waveguide PMS is integrated with a three-waveguide "shortcut to adiabaticity" structure, we realize a broadband, high splitting-ratio (η_c) mode splitter for spatial separation of TE- (H-) polarized pump (700-850 nm for η_c>99%), TM- (V-) polarized signal (1510-1630 nm for η_c>97%), and TE- (H-) polarized idler (1480-1650 nm for η_c>97%) modes. Such a unique integrated-optical device is of potential for facilitating the on-chip implementation of a pump-filtered, broadband tunable entangled quantum-state generator.

1. Introduction

Optical waveguides are essential elements for constructing integrated optical circuits and devices. In particular, the mechanism and effect of evanescent coupling between waveguides has been widely utilized to realize many interesting photonic devices useful in integrated optics including directional couplers. Directional couplers perform optical power exchange between usually two closely lying waveguides via the access of this evanescent effect, sensitive to the wavelength and polarization because of the dispersive nature of such mode interference couplers. They found many applications in, e.g., wavelength multiplexers/demultiplexers and polarization splitters [1–3]. On the other hand, the study of waveguide couplers working with broad spectral bandwidth has been in demand for important applications in especially optical communication and networking systems (for such as power or mode division, exchange, or switch [4–6]). In particular, the development of broadband polarization splitters has received much attention as wavelength-independent polarization control has become an important optical processing function in integrated optical and emerging quantum optical circuit technologies [7–9]. Several waveguide architectures have been proposed to implement integrated-optic polarization splitters for working in a broad spectral band [9–12] and many of them have been demonstrated in substrates such as

semiconductors and silica (and the incorporation of both into such as silicon-on-insulator materials) [10,13,14]. These materials, though supporting the construction of devices in highly compact integrated forms, are convenient only for building passive components, which could largely reduce their roles in developing on-chip optical circuits usually comprising active and (quadratically) nonlinear functional devices such as frequency mixers, modulators, and switches for, e.g., optical networking and communication and quantum information applications. $LiNbO_3$, renowned as "the silicon of photonics", has been long a popular (and perhaps the most important) material for building various integrated optical circuits/devices (reviews of the recent development in $LiNbO_3$ photonics can be found in [15–17]) because of its versatility derived from its excellent electro-optic (EO), acousto-optic, nonlinear-optic (NLO), and piezoelectric properties with wide optical transparent range (~0.4-5 μm) [18]. It will thus be interesting and desirable to develop a broadband polarization splitter in $LiNbO_3$.

Polarization splitters have been implemented in $LiNbO_3$ waveguides [19–21]. These schemes were usually based on a Y-branch waveguide configuration (few were based on EO controlled waveguide directional couplers [22]) and can show high polarization extinction ratios (PER) through the creation or engineering of an asymmetric/heterogeneous splitting structure to enhance the modal birefringence [19–21]. However, an increased birefringence usually results in an increased dependence of the mode-splitting efficiency on wavelength, limiting the operation bandwidth of the devices. Besides, the implementation of these high PER devices relies on a careful engineering of the waveguide configuration or more often involves a more complex fabrication procedure (such as those for heterogeneous splitters). Recently, we have successfully demonstrated broadband and high coupling-efficiency directional couplers in three-waveguide systems in $LiNbO_3$ [23] based on a peculiar light transfer behavior analogous to a counterintuitive adiabatic tunneling effect discovered in quantum physics [24–26]. In [23], two standalone adiabatic couplers with different structure parameters have been derived for working with the TE and TM polarization modes, respectively. Calculated coupling bandwidths of ~50 and ~200 nm in the 1.5-μm telecom band at a cross-coupling efficiency (η_c) of >97% were obtained in the two 5-cm-long $LiNbO_3$ three-waveguide adiabatic directional couplers for fundamental TE and TM polarization modes, respectively. The straightforward idea of combining the two three-waveguide adiabatic directional couplers in a monolithic $LiNbO_3$ chip to build a broadband high-PER (defined here as a PER>17 dB) polarization mode splitter (PMS) is actually not viable. The challenge is that the two devices work optimally only for the respective design polarization and unwanted cross talk can happen due to the presence of another polarization mode. A more sophisticated adiabatic waveguide system is thus required to achieve a polarization splitter advantageous over existing splitters using conventional mechanisms. In our previous study, we have implemented a unique adiabatic waveguide splitter in $LiNbO_3$ whose polarization splitting ratio (PSR) is wavelength dependent for the application in quantum-polarization state preparation [27]. However, the high-PSR bands of the device do not overlap for the two cross-polarized modes, by definition it is not a PMS. In this work, we demonstrate the first broadband polarization splitter based on the adiabatic directional coupling mechanism in $LiNbO_3$. The adiabatic waveguide scheme of the PMS has resembled that reported in [27] but been realized with a modified dispersion and adiabaticity conditions. The unique device exhibits a bandwidth of ~140 nm at PER of >20 dB and >18 dB for the TE- and TM-polarized modes, respectively, which could be the record broad bandwidth in $LiNbO_3$ based PMSs. The advance of adiabatic coupler technology in the $LiNbO_3$ platform creates advantageous photonic elements that are featured by high fabrication tolerance, high power coupling efficiency, and broad operational bandwidth, beneficial to readily apply them to, e.g., integrated optical and quantum photonic circuits on a chip (see below and [28] as potential application examples).

2. Device design and performance simulation

The methodology used in this work for the study and design of an adiabatic waveguide system builds on the approach presented in our previous report [23]. The optimum structure parameters of the coupled waveguides are first determined according to the adiabatic conditions (refer to Eqs. (2) and (3) in [23]) to realize a system with high adiabaticity (the process is termed here as "adiabaticity engineering"). The configuration is then confirmed by numerically examining the mode evolution in the system using the "Beam Propagation Method" (BPM) [29]. In this work, the adiabatic coupler systems working across the telecom S, C, and L bands are constructed based on Ti-diffused *z*-cut $LiNbO_3$ (Ti:$LiNbO_3$) waveguides, which are the most widely used ones for supporting both TE and TM polarized modes with low propagation losses [30]. Through the study, we found no adiabatic coupling configurations in three-waveguide (the simplest) schemes in $LiNbO_3$ that can work as a high-PER polarization mode splitter (i.e., no three-waveguide schemes can have proper adiabaticity for achieving a high cross-coupling of one polarization mode while permitting a high straight-through transmission of the other polarization mode). The result can be attributed to the insufficient birefringence in $LiNbO_3$ in this spectral region (Δn<0.08). Instead of resorting to the enhancement of the modal birefringence, we followed the adiabaticity engineering methodology and found that an arrayed waveguide structure with three (slash) intermediate waveguides can provide a highly polarization-dependent adiabaticity of the light transfer between two (straight) outer waveguides and facilitate the realization of a broadband PMS. An odd number of intermediate waveguides is used for achieving an ideally complete power transfer in an optical adiabatic passage process, an analogue of the mechanism of the dressed states [31] in the stimulated Raman adiabatic passage (STIRAP) process [24] found in the quantum system. Though the polarization-dependent adiabaticity and therefore the PER of the device can be possibly enhanced with the increase of intermediate waveguide number (as it provides more structure parameters to manipulate to optimize the adiabaticity engineering process), the increase of waveguide number will also complicate the design process and the overall system configuration. Besides, additional waveguides will inevitably introduce additional loss in the light transfer process of finite efficiency among waveguides.

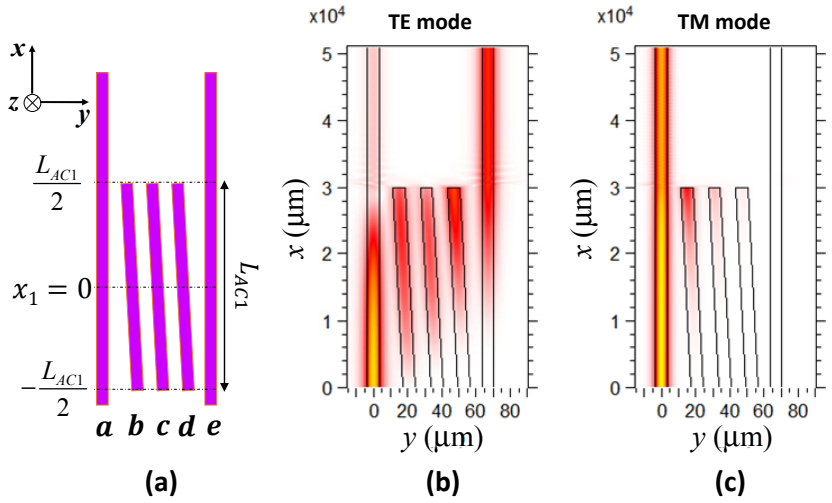

Fig. 1. (a) Schematic configuration of a five-channel-waveguide adiabatic coupler built in Ti:$LiNbO_3$ as a broadband polarization mode splitter. (b) and (c) Simulated evolutions of the wave intensity in such a five-waveguide adiabatic coupler system for TE- and TM-polarized 1550-nm fundamental modes initially excited in waveguide ***a***, respectively.

Figure 1(a) shows the schematic configuration of such a five-channel-waveguide structure built in Ti:$LiNbO_3$. The structure forms an adiabatic directional coupler for the fundamental TE-polarized mode where significant power coupling of the mode can occur from the input (straight) waveguide ***a*** to the outmost (straight) waveguide ***e*** (far away from the evanescent distance of the waveguide ***a***) mediated via three slash waveguides ***b***, ***c***, and ***d***, while the fundamental TM-polarized mode will just go straight through the waveguide ***a***. The scheme thus forms a polarization mode splitter (TE- and TM-polarized modes are spatially separated and exit from the waveguides ***e*** and ***a***, respectively). In our current methodology, we found that no waveguide configuration in $LiNbO_3$ could be found in this spectral region for achieving the adiabatic tunneling of only the TM-polarized mode without significant power coupling of the TE-polarized mode from waveguide ***a*** to waveguide ***e***. Such a limitation is due to the polarization-dependent mode characteristics in Ti:$LiNbO_3$ waveguides (one major effect is that the mode size of the TE-polarized mode is about 1.46 times larger than that of TM-polarized mode). In Fig. 1(a), L_{AC1} = 30 mm is the effective length of the five-waveguide coupler system (referred to as ***AC*1** system). The three slash intermediate waveguides are identical and have the same inclination. $S_{ij}(x)$ is the distance between the inner-edges of the waveguides i and j at x_1 (x_1 is the distance along the wave propagation direction with x_1 = 0 being in the middle of the ***AC*1** system). Specifically, $S_{ab}(-L_{AC1}/2)$ = 14 μm, $S_{ab}(L_{AC1}/2)$ = 8 μm, $S_{bc}(\pm L_{AC1}/2) = S_{cd}(\pm L_{AC1}/2)$ = 9 μm, $S_{de}(-L_{AC1}/2)$ = 7 μm, $S_{de}(L_{AC1}/2)$ = 13 μm, and S_{ae} = 60 μm, $\Delta S_k = S_{ak}(-L_{AC1}/2)-S_{ak}(L_{AC1}/2)$, where the subscript k denotes the intermediate waveguide ***b***, ***c***, or ***d***, among them ΔS_b = 6 μm. All the waveguides have the same width of w_{AC1} = 7 μm. These structure parameters are derived first via the adiabaticity engineering method and can be optimized/confirmed via the performance simulation as aforementioned. As a result, a relationship between the coupling coefficients (denoted as $\kappa_{i,j}$ for coupling between waveguides i and j) of the two polarization modes, $\kappa_{ab}^{TM} < \kappa_{ab}^{TE} < \kappa_{bc}^{TE}$, can be attained to effectively reduce the tunneling probability of the TM wave, while on the other hand a slow adiabatic light-transfer condition for the TE wave can be satisfied (where an adiabatic parameter (or adiabatic rate) $\gamma \equiv \Delta S_b/\kappa_0 r L_{AC1} \sim 0.16 << 1$ is obtained for the TE wave. Since the coupling and the waveguide characteristic parameters for the two modes satisfy the relationships: $\kappa_0^{TE} > \kappa_0^{TM}$ and $r^{TE} > r^{TM}$, it leads to a desired relationship for the adiabaticity: $\gamma^{TE} < \gamma^{TM}$; refer to [23] for the detailed information).

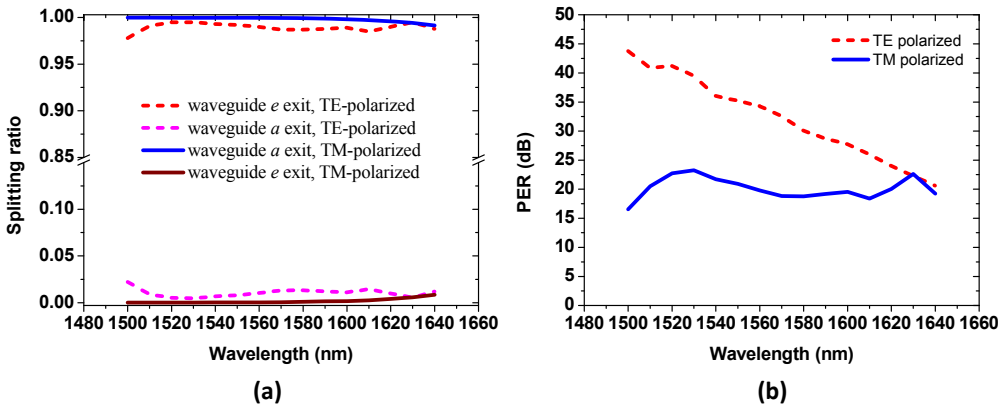

Fig. 2. Calculated (a) splitting ratio and (b) PER of the five-waveguide PMS as a function of the excitation wavelength for both TE- and TM-polarized fundamental modes.

Figures 1(b) and 1(c) show the simulated evolutions of the wave intensity in such a five-waveguide adiabatic coupler system for TE- and TM-polarized 1550-nm fundamental modes initially excited in waveguide ***a***, respectively, using the BPM technique. In the calculation, we

have assumed the propagation constants of the straight waveguides ***a*** and ***e*** are the same (i.e., $\beta_a = \beta_e$) as well as those for the slash waveguides ***b***, ***c***, and ***d*** ($\beta_b = \beta_c = \beta_d$) and the coupling coefficients of neighboring waveguides are the same (i.e., $\kappa_{i,i+1}(x_1) = \kappa_{i+1,i}(x_1)$) according to our design. The results clearly show the TE-polarized mode exhibits wave evolution dynamics as expected in a typical adiabatic light passage system, where the vast majority of the output power has been obtained from the waveguide ***e*** (with a splitting ratio of ~99.2%) with slight excitation of the intermediate waveguides. In the meantime, the TM-polarized mode transmits through waveguide ***a*** with a power splitting ratio of ~99.9%. The resultant PER, defined as $r_{TE} = 10\log(P_e^{TE} / P_e^{TM})$ and $r_{TM} = 10\log(P_a^{TM} / P_a^{TE})$ for TE- and TM-polarized modes, respectively, when a wave in 45° polarization state is input, where P_e and P_a are the output powers obtained from waveguides ***e*** and ***a***, respectively, are r_{TE} = 35.2 dB and r_{TM} = 20.9 dB at 1550 nm. Figures 2(a) and 2(b) show the calculated splitting ratio (for a purely TE- or TM-polarized input wave) and PER of the five-waveguide PMS (Fig. 1(a)) as a function of the excitation wavelength, respectively, for both TE- and TM-polarized fundamental modes. It can be found that a bandwidth of ~140 nm for the TE- (TM-) polarized mode at a high PER of >20 dB (>18 dB) and (at the same time) a high splitting ratio of >98% (>99%) can be achieved in this unique Ti:$LiNbO_3$ PMS, which is to the best of our knowledge the broadest bandwidth ever reported in integrated optical $LiNbO_3$ polarization mode splitters.

The total losses of the five-waveguide PMS are ~2.8 dB and ~1.3 dB for the TE- and TM-polarized modes, respectively, according to the BPM simulation. In particular, it shows a certain amount of power is lost at the ends of the intermediate waveguides (see Figs. 1(b) and 1(c)). The loss can be further minimized by increasing the adiabaticity of the waveguide system via, e.g., using a longer effective coupler length (L_{AC1}) as suggested in our previous study for three-waveguide adiabatic coupling systems [23]. Here we limit our study to L_{AC1} = 30 mm to allow the device to integrate with another adiabatic coupler to form a three-port mode splitter for quantum photonic applications in a reasonable total device length (see below).

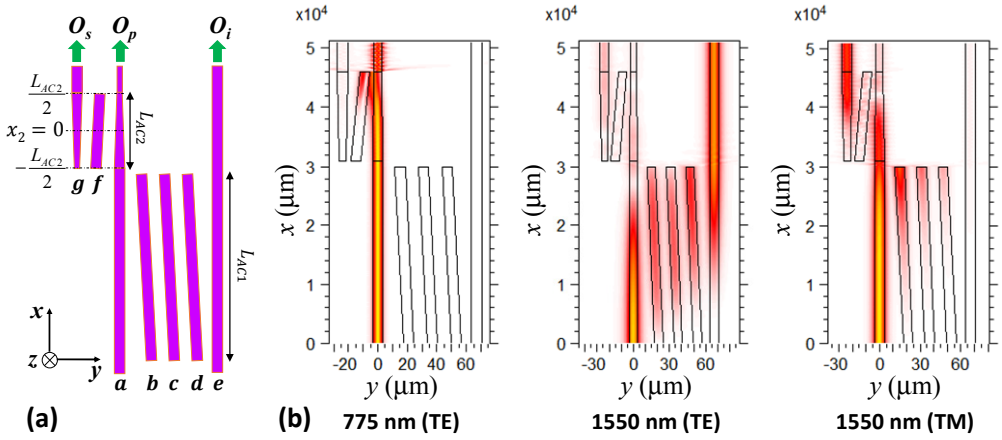

Fig. 3. (a) Schematic of the integrated adiabatic waveguide polarization mode-splitter (IAPMS) device. (b) Simulated evolutions of the wave intensity in the IAPMS for TE (or H)-polarized pump at 775 nm, TM (or V)- and TE (or H)-polarized signal and idler waves at 1550 nm.

We further demonstrate that such a high-performance integrated broadband and high-PER polarization splitter can be applied to facilitate the on-chip generation of entangled quantum states. In our previous study, we have developed a mode splitter whose PSR is wavelength dependent, used for spatial splitting of the cross-polarized, nondegenerate signal and idler pair

photons generated in a type-II spontaneous parametric down conversion (SPDC) process, in which different quantum polarization-path states can be prepared [27]. However, among the states, an entangled Bell state can only be produced at a specific splitting ratio (50%/50%), and besides, it increases the difficulty of building an efficient timing-compensation mechanism in the device when operated at this non-polarizing splitting condition as both polarization modes are split equally into two paths. In this work, we further propose a waveguide scheme similar to that in [27] but instead working as an on-chip achromatic (wavelength-independent), high-PER polarization mode splitter in the telecom bands for implementing a broadband tunable Bell state generator.

Table 1. Summary of the structure and fabrication parameters of the devices developed in this work and in [27]

Device	Design target	Structure-Adiabaticity						Fabrication-Dispersion		
		Based on an integrated five-waveguide (with three slash intermediate waveguides) and three-waveguide (with two taper outer waveguides) adiabatic coupling structure								
		Key structure parameters (at $L_{AC1}/2$) (μm)				Adiabatic parameters (at 1.55 μm)		Ti-layer thick-ness (nm)	Mode index change	
		S_{ab}	$S_{bc} = S_{cd}$	S_{de}	S_{ae}	γ_{TE}	γ_{TM}		Δn_e	Δn_o
Ref [27].	A wavelength- and polarization-dependent adiabatic coupling device	11	10	14	67	0.32	0.45	90	0.0119	0.0052
									$\Delta n_e/\Delta n_o = 2.29$	
This study	A broadband, high PER adiabatic polarization-mode splitter	8	9	13	60	0.16	0.23	130	0.0159	0.0089
									$\Delta n_e/\Delta n_o = 1.79$	

We found the splitting spectra of the waveguide system studied in [27] (showing high-PSR bands do not overlap for the two polarization modes) can be modified via the adiabaticity and dispersion engineering techniques (as discussed in the sections 2 and 3). The engineering modifies the modal properties in the waveguide system, leading to the realization of the first and a genuine broadband PMS in $LiNbO_3$ (where the two cross-polarized modes now work in the same band broadly spanning telecom S, C, and L bands with high PER, see Fig. 6 below). Table 1 lists the structure and fabrication parameters of the devices developed in this work and in [27] for a more explicit comparison. It also shows a better adiabaticity and a less modal birefringence have been obtained with the device studied in this work for reaching an increased PER and bandwidth. Figure 3(a) shows the schematic of such a waveguide system in Ti:$LiNbO_3$ that integrates two adiabatic directional couplers with one in the front section being exactly the five-waveguide structure (***AC*1**) shown in Fig. 1(a) and the other one located downstream being a three-waveguide adiabatic passage structure (***AC*2**). ***AC*2** is used to further spatially transfer the TM-polarized wave transmitted from ***AC*1** through waveguide ***a*** to the outer waveguide ***g*** mediated by single slash waveguide ***f***. In ***AC*2**, the two outer waveguides are tapered in opposite direction to effectively shorten the adiabatic coupling length (L_{AC2} = 15 mm), as suggested by the "shortcut to adiabaticity" technique [32], for reducing the total length of the device. An interesting comparison can be made to a 50-mm long, three-waveguide adiabatic coupler built in Ti:$LiNbO_3$ reported in [23] without using the taper waveguide design. The output characteristic (see power splitting spectrum in Fig. 7(d) in [23]) of this 50-mm long device for TM-polarized mode has resembled that obtained with the 15-mm long ***AC*2** (see Fig. 6(b) below), implying a length reduction of a factor of 3.3 can be achieved using the "shortcut to adiabaticity" design. The tapering rate

used in ***AC2*** is $(w_{AC1}\text{-}w_{AC2})/L_{AC2}$, where w_{AC2} = 5 μm. The corresponding propagation constants of the waveguides ***a*** and ***g*** in ***AC2*** then vary per the taper structure as $\beta_a(x_2) = \beta_a\text{-}(x_2 + L_{AC2}/2)\delta\beta$ and $\beta_g(x_2) = \beta_a + (x_2\text{-}L_{AC2}/2)\delta\beta$, respectively, where x_2 is the distance along the wave propagation direction with $x_2 = 0$ being in the middle of the ***AC2*** system and $\delta\beta$ is the gradient of the propagation constant formed in the taper waveguides. Other structure parameters are: $S_{af}(\text{-}L_{AC2}/2) = 8$ μm, $S_{af}(L_{AC2}/2) = 3$ μm, $S_{fg}(\text{-}L_{AC2}/2) = 3$ μm, and $S_{fg}(L_{AC2}/2) = 8$ μm. We don't apply the taper design to ***AC1*** for adiabatic light transfer of the TE-polarized mode because we found it would lead to a high propagation loss in the taper structure due to the relative large mode size of the TE-polarized mode (which is 1.46 times larger than the TM-polarized mode as aforementioned).

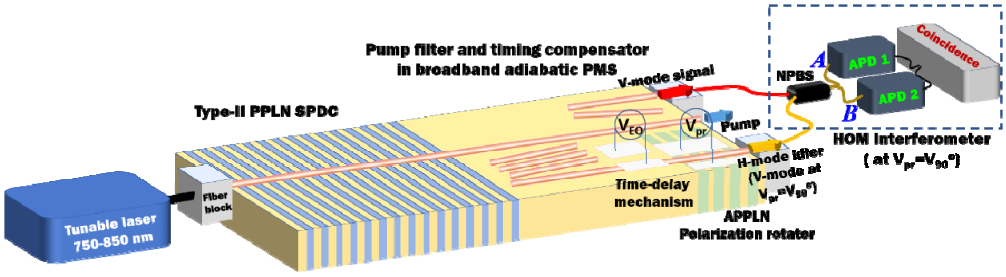

Fig. 4. Schematic of a pump-filtered, broadband tunable Bell-state generator based on the on-chip integration of the IAPMS with a type-II PPLN SPDC pumped by a laser tunable around 775 nm.

The integrated adiabatic waveguide polarization mode-splitter (IAPMS) device shown in Fig. 3(a) can be further integrated with a type-II periodically poled lithium niobate (PPLN) SPDC pumped by a laser tunable around 775 nm (see Fig. 4). The system then works as a pump filter in combination with a signal and idler (cross-polarized) mode splitter for doing timing compensation on chip over a broad band. In our design, the residual pump wave will transmit through waveguide ***a*** and exit at port $\boldsymbol{O_p}$, while the TM- and TE-polarized (signal and idler) waves will adiabatically tunnel to waveguides ***g*** and ***e*** and exit at ports $\boldsymbol{O_s}$ and $\boldsymbol{O_i}$, respectively. Though conventional directional couplers can be used to separate the pump wave (shorter wavelength mode) from the signal/idler wave (longer wavelength mode), they usually suffer from the low fabrication tolerance and limited working bandwidth (i.e., sensitive to the working wavelength) as we have discussed in the Introduction section, hindering them from being a practical element for building an on-chip system like the one shown in Fig. 4 for a broadband tuning application. The simulated evolutions of the wave intensity in such an integrated adiabatic waveguide mode-splitter system (for TE (or H)-polarized pump at 775 nm, TM (or V)- and TE (or H)-polarized signal and idler waves at 1550 nm) are shown in Fig. 3(b). The timing-compensation mechanism can be built in the downstream section of the waveguide ***e*** (see Fig. 4) using e.g., the EO group-index modulation method; the IAPMS device could thus be an on-chip solution of a bulky free-space timing compensator based on an optical delay line after a polarization beam splitter [33,34]. Because the proposed integrated device features high pump, signal, and idler splitting ability, the purity of the generated photon-pair states can be maintained for approaching maximal entanglement [35].

3. Device fabrication and output performance characterization

We fabricated the IAPMS device (Fig. 3(a)) in a 51-mm long, 10-mm wide, and 0.5-mm thick *z*-cut $LiNbO_3$ chip. The derived architecture of the waveguide system was first constructed by a Ti strip layer of a thickness of 130 nm over the -*z* surface of the chip. Ti:$LiNbO_3$ waveguides were then formed by performing the thermal indiffusion process to the sample in a 3-zone furnace at 1035°C for 12 hours under a Li_2O rich circumstance (application of

$LiNbO_3$ powder) and a constant oxygen flow [36]. In this work, the modal dispersion has been engineered via the adjustment of the diffusion condition (mainly the Ti-layer thickness) to achieve proper modal properties (mode sizes and indices) derived with the aid of the BPM for implementing a broadband, high PER PMS in Ti:$LiNbO_3$ waveguides. The resultant refractive index profiles are with surface index changes of $\Delta n_o = 0.00893$ and $\Delta n_e = 0.01592$ and e^{-1} depths of $d_o = 5.0$ μm and $d_e = 5.12$ μm (derived by a prism coupler [37] at 532 nm) for the guiding of single TE and TM (fundamental) modes in a 7-μm-wide channel waveguide in the spectral range 1400-1700 nm. One of the important features of adiabatic couplers is their high tolerance to the fabrication errors. Figure 5 shows the calculated splitting ratios obtained from the three output ports $\boldsymbol{O_s}$, $\boldsymbol{O_i}$, and $\boldsymbol{O_p}$ of the integrated adiabatic waveguide device as a function of the waveguide depth for the input of a 1550-nm TM-polarized wave, respectively. The output results of a typical heterogeneous Y-branch polarization mode splitter with one arm made by Ti diffused waveguide and the other arm made by proton-exchanged waveguide, an analogue of that studied in [20], are also calculated for comparison. It clearly shows the adiabatic waveguide device can have much higher fabrication tolerance where a splitting ratio of >97% at TM arm ($\boldsymbol{O_s}$) can be maintained over a large variation of the fabrication-dependent waveguide depth of from 5.1 to 6.0 μm (which is 5.36-5.53 μm for the Y-branch scheme).

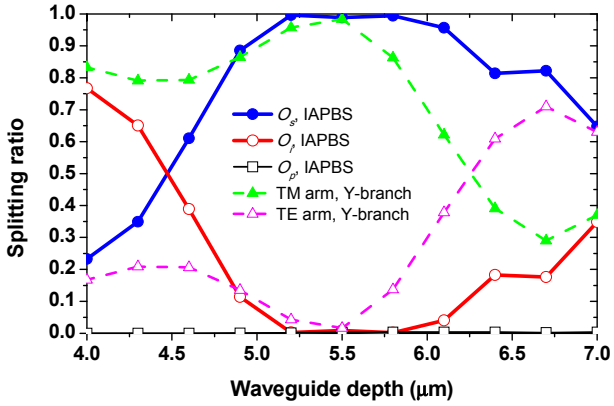

Fig. 5. Calculated splitting ratios obtained from the three output ports $\boldsymbol{O_s}$, $\boldsymbol{O_i}$, and $\boldsymbol{O_p}$ of the IAPMS device and the two arms of a typical heterogeneous Y-branch PMS as a function of the waveguide depth for the input of a 1550-nm TM-polarized wave.

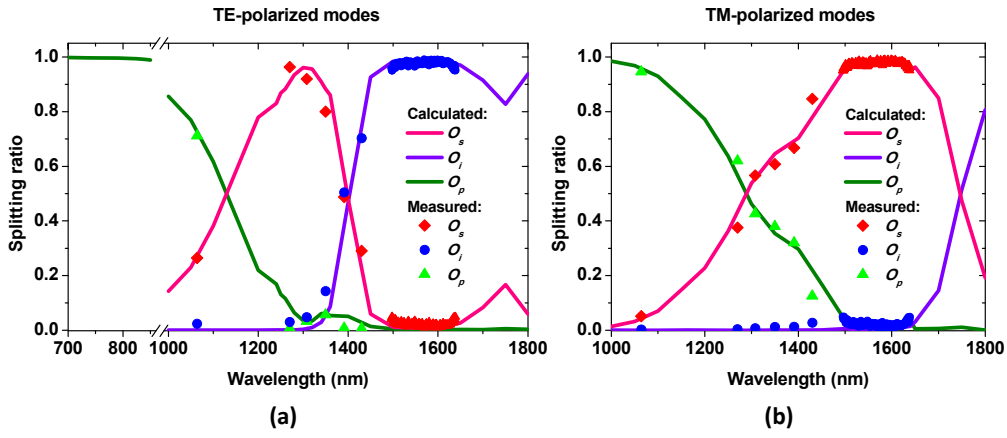

Fig. 6. Measured and calculated normalized output powers from the three output ports of the $LiNbO_3$ IAPMS as a function of wavelength for (a) TE- and (b) TM-polarized modes.

The measurement of the fabricated IAPMS device was performed in an optical testbed using a linearly-polarized external cavity laser (ECL) tunable between 1495 and 1640 nm as the light source and a photodetector and an infrared CCD as the output power and mode profile measurement system (the testbed is basically identical to that employed in [23]). An input power of <~1 mW was used. Figures 6(a) and 6(b) show the measured and calculated normalized output powers (normalized to the total output power) from the three output ports (i.e., the splitting ratios) of the $LiNbO_3$ IAPMS as a function of wavelength (1000-1800 nm) for TE- and TM-polarized modes, respectively. The experimental data outside the ECL tuning range were obtained with distributed feedback laser diodes of different wavelengths. The measured data are in good agreement with the simulation prediction, showing a high splitting efficiency (>97%) over a broad bandwidth of >120 nm (1510-1630 nm) and >170 nm (1480-1650 nm) for the TM and TE polarization modes, respectively. Figure 7 shows the captured output mode intensity profiles from the device for several different excitation wavelengths. Moreover, the unique device has a broad transmission band for the TE-polarized pump throughout the waveguide ***a*** (>99% splitting efficiency between 700 and 850 nm), as the calculated data shown in Fig. 6(a).

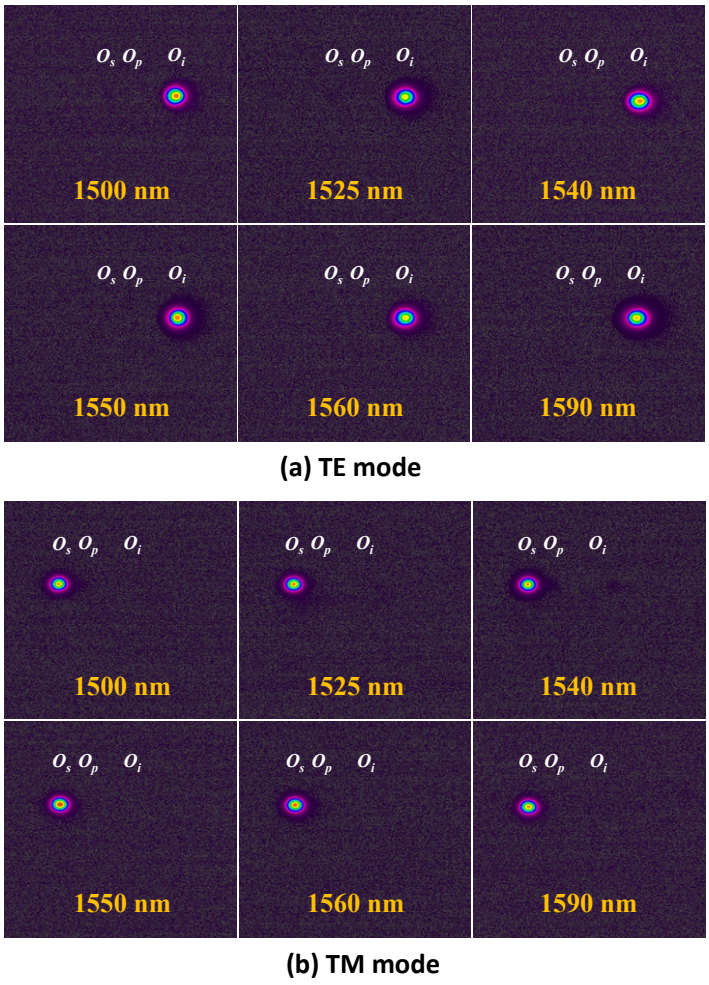

Fig. 7. Captured output mode intensity profiles from the device for several different excitation wavelengths.

4. Potential applications in quantum photonics

The results obtained above imply that a broadband tunable Bell-state generator can be realized with the system shown in Fig. 4. An important advantage is that the generated (degenerate) signal and idler pair photons (V- and H-polarized modes) and the corresponding H-polarized pump wave from the type-II PPLN SPDC source can now be processed in a spectral band within the broad working bandwidth of the IAPMS device (Fig. 6). The polarization-entangled states,

$$\left|\Psi^{\pm}\right\rangle = \frac{1}{\sqrt{2}}\left(\left|H_A(\lambda)\right\rangle\left|V_B(\lambda)\right\rangle \pm e^{i\varphi}\left|V_A(\lambda)\right\rangle\left|H_B(\lambda)\right\rangle\right) \tag{1}$$

(where the subscripts A and B label the photons entering the paths ***A*** and ***B*** after the non-polarizing beam splitter (NPBS) in the coincidence measurement setup and φ is the relative phase between the two states. Here $\varphi = 0$ is presupposed for a maximally-entangled Bell state) can be generated (probabilistically (50%) [34]) in signal/idler wavelength ($\lambda = \lambda_s = \lambda_i$ for degenerate process) range from 1520 nm to 1560 nm, tunable via the pump wavelength (from 760 nm to 780 nm) and the quasi-phase-matched condition (via, e.g., temperature from 20°C to 220°C) of the PPLN (with a grating period of 9.4 μm) SPDC section. The non-classicality of the source can be confirmed by a Hong–Ou–Mandel (HOM) interferometer [38] whose functionality can be enabled in the system shown in Fig. 4 by applying a proper voltage ($V_{pr} = V_{90^o}$) to the aperiodically poled lithium niobate (APPLN) EO polarization mode converter (PMC) [36,39] built in a section downstream of the timing compensator located in one output arm of the IAPMS. An APPLN has been used to implement muti-/broad-band devices [39]. The PMC works as an on-chip polarization rotator, when driven at V_{90^o}, it will rotate the polarization mode of the idler (here TE polarized) to be identical to the signal mode (TM polarized) to perform the interference measurement. Furthermore, the broadband IAPMS device also benefits the on-chip implementation of non-degenerate polarization-entangled quantum light sources producing

$$\left|\Psi\right\rangle = \frac{1}{\sqrt{2}}\left(\left|H_{\lambda_s}\right\rangle\left|V_{\lambda_i}\right\rangle + e^{i\varphi}\left|V_{\lambda_s}\right\rangle\left|H_{\lambda_i}\right\rangle\right) \tag{2}$$

or

$$\left|\Psi\right\rangle = \frac{1}{\sqrt{2}}\left(\left|H_{\lambda_s}\right\rangle\left|H_{\lambda_i}\right\rangle + e^{i\varphi}\left|V_{\lambda_s}\right\rangle\left|V_{\lambda_i}\right\rangle\right) \tag{3}$$

states based on a type-II cascaded/integrated PPLN SPDC source designed for producing two non-degenerate photon pairs with one in a $\left|HV\right\rangle$ state and the other in a $\left|VH\right\rangle$ state [40] or a type-0 and type-I cascaded/integrated PPLN SPDC source designed for producing two non-degenerate photon pairs with one in a $\left|HH\right\rangle$ state and the other in a $\left|VV\right\rangle$ state, respectively. Since the determination of the non-degenerate wavelengths (λ_s and λ_i) of the photon pairs are simultaneously subject to two quasi-phase-matching conditions of the two down-conversion processes, the wavelengths λ_s and λ_i could be found to be far apart in spectrum even in two ends of a telecom band [40]. The IAPMS device demonstrated in this work, having a working bandwidth spanning telecom S, C, and L bands, has thus a great advantage of being ready to integrate and work with such non-degenerate SPDC sources; in other words, the device supports (or accommodates to) the versatile design of the SPDC sources built in $LiNbO_3$ waveguide platform because of its broad bandwidth. In this non-degenerate source scheme, the quantum entangled states can be generated and tested in the system shown in Fig. 4 with the NPBS in the HOM interferometer (operated at $V_{pr} = V_{90^o}$) being replaced by a dichroic mirror for a deterministic splitting of the non-degenerate photons by wavelength [40].

Table 2 summarizes the output characteristics, built-in functions, and range of the quantum photonic applications of the IAPMS studied in this work. The relevant information of the polarization- and wavelength-dependent mode splitter presented in [27], interesting for different quantum-polarization states preparation, is also list for the comparison.

Integrated robust broadband tunable Bell-state generators are of great potential for a wide range of applications in quantum photonics. Having access to a high quality photon-pair source will allow experimental tests of novel concepts, such as devices designed for quantum tomography [41,42], quantum state manipulation and storage [43], quantum state in-line reconstruction [44], quantum mechanics tests [45] and many others [46]. Tunability makes this source extremely versatile, while broadband operation gives the option to select the right output wavelengths for the task. Broadband performance also means that this concept is tolerant to minor fabrication imperfections. Finally, polarization splitting allows using the device for both path-encoded and polarization-encoded state generations, unlike previous implementations not supporting this feature [47].

Table 2. Summary of the output characteristics, built-in functions, and range of the quantum photonic applications of the devices studied in this work and in [27]

Device	Output characteristics			Quantum photonic applications	
	Mode	Splitting spectrum		Built-in functions	Application range
		Description	Bandwidth (PSR>97%)		
Ref [27].	TE	High polarization-splitting ratio (PSR) bands do not overlap for the two cross-polarized modes	~70 nm (1600-1670 nm)	1. Pump filtering. 2. Wavelength-dependent polarization splitting ratio. 3. 50%/50% non-polarizing beam splitting (narrowband). 4. EO timing compensation (less efficient).	Working with non-degenerate type-II SPDC sources for quantum-polarization states preparation
	TM		~90 nm (1425-1515 nm)		
This study	TE	Both cross-polarized modes work in a band broadly spanning telecom S, C, and L bands with high PSR	~170 nm (1480-1650 nm)	1. Pump filtering. 2. Broadband (achromatic) polarization-mode splitting. 3. EO timing compensation. 4. EO polarization rotation.	Working with type-0/-I/-II nondegenerate/degenerate sources for broadband tunable Bell state generation
	TM		~120 nm (1510-1630 nm)		

The core $LiNbO_3$ chip (integrating a 20-mm long PPLN SPDC source and a 51-mm long IAPMS) in the pump-filtered, broadband tunable Bell-state generator schematically shown in Fig. 4 can be implemented in a 3" or 4" commercially available $LiNbO_3$ wafer. To effective reduce the structure length of the on-chip $LiNbO_3$ photonic devices demonstrated in this study, some emerging materials such as the thin-film lithium niobate-on-insulator (LNOI) could be of potential interest, as the material is possible to achieve a high adiabaticity for the passage of light in a much smaller footprint size (typical LNOI device is on the order of few mm^2) [48] due to its high index-contrast waveguide structure. Compact adiabatic couplers have been demonstrated in CMOS-compatible materials [49], though their on-chip compatibility with active/nonlinear photonic devices (such as EO modulators and SPDC sources) still remains an issue as discussed in the Introduction section.

5. Conclusion

We have designed and constructed a broadband integrated adiabatic waveguide system (the IAPMS system) cascading a five-waveguide (with three slash intermediate waveguides) and a three-waveguide (with two taper outer waveguides) structures for performing adiabatic light transfer of TM- and TE-polarized (signal and idler) fundamental modes to two different output ports in a broad bandwidth of >120 nm (1510-1630 nm) and >170 nm (1480-1650 nm), respectively, at a high splitting efficiency of >97%. Besides, TE-polarized modes in the (pump) band from 700 to 850 nm can transmit straight-through the IAPMS to the third port at a high splitting efficiency of >99%. The results characterized from the device are in good agreement with the simulation prediction. The unique device can be attractive for applications in integrated optical and quantum optical circuits. In particular, it can be further integrated with PPLN SPDC sources, where the IAPMS can act as an on-chip pump filter, signal and idler mode splitter, timing compensator, and polarization rotator for facilitating the building of a broadband tunable polarization-entangled Bell-state generator.

Funding

Ministry of Science and Technology of Taiwan (MOST) (106-2221-E-008-068-MY3, 107-2911-I-008-501, 107-2627-E-008-001, and 104-2923-E-007-001-MY4); German Academic Exchange Service (Project-ID 57334258); Australia-Germany Joint Research Cooperation Scheme.

References

1. H. C. Cheng and R. V. Ramaswamy, "Symmetrical directional coupler as a wavelength multiplexer-demultiplexer: theory and experiment," IEEE J. Quantum Electron. **27**(3), 567–574 (1991).
2. D. Gu, O. Eknoyan, and H. F. Taylor, "Polarization dependence in Ti-diffused $LiNbO_3$ directional couplers," Appl. Opt. **41**(1), 74–77 (2002).
3. S. Soudi and B. M. A. Rahman, "Design of a compact polarization splitter by using identical coupled silicon nanowires," J. Lightwave Technol. **34**(17), 4169–4177 (2016).
4. G. F. R. Chen, J. R. Ong, T. Y. L. Ang, S. T. Lim, C. E. Png, and D. T. H. Tan, "Broadband Silicon-On-Insulator directional couplers using a combination of straight and curved waveguide sections," Sci. Rep. **7**(1), 7246 (2017).
5. K. J. Park, K. Y. Song, Y. K. Kim, J. H. Lee, and B. Y. Kim, "Broadband mode division multiplexer using all-fiber mode selective couplers," Opt. Express **24**(4), 3543–3549 (2016).
6. S. Chen, Y. Shi, S. He, and D. Dai, "Low-loss and broadband 2 × 2 silicon thermo-optic Mach-Zehnder switch with bent directional couplers," Opt. Lett. **41**(4), 836–839 (2016).
7. L. T. Feng, M. Zhang, Z. Y. Zhou, M. Li, X. Xiong, L. Yu, B. S. Shi, G. P. Guo, D. X. Dai, X. F. Ren, and G. C. Guo, "On-chip coherent conversion of photonic quantum entanglement between different degrees of freedom," Nat. Commun. **7**(1), 11985 (2016).
8. G. Huang, T. H. Park, and M. C. Oh, "Broadband integrated optic polarization splitters by incorporating polarization mode extracting waveguide," Sci. Rep. **7**(1), 4789 (2017).
9. C.-L. Zou, F.-W. Sun, C.-H. Dong, X.-F. Ren, J.-M. Cui, X.-D. Chen, Z.-F. Han, and G.-C. Guo, "Broadband integrated polarization beam splitter with surface plasmon," Opt. Lett. **36**(18), 3630–3632 (2011).
10. S. Lin, J. Hu, and K. B. Crozier, "Ultracompact, broadband slot waveguide polarization splitter," Appl. Phys. Lett. **98**(15), 151101 (2011).
11. D. Dai and J. E. Bowers, "Novel ultra-short and ultra-broadband polarization beam splitter based on a bent directional coupler," Opt. Express **19**(19), 18614–18620 (2011).
12. J. Wang, B. Niu, Z. Sheng, A. Wu, W. Li, X. Wang, S. Zou, M. Qi, and F. Gan, "Novel ultra-broadband polarization splitter-rotator based on mode-evolution tapers and a mode-sorting asymmetric Y-junction," Opt. Express **22**(11), 13565–13571 (2014).
13. H. Wu, Y. Tan, and D. Dai, "Ultra-broadband high-performance polarizing beam splitter on silicon," Opt. Express **25**(6), 6069–6075 (2017).
14. M. Olivero and M. Svalgaard, "Direct UV-written broadband directional planar waveguide couplers," Opt. Express **13**(21), 8390–8399 (2005).
15. W. Sohler, H. Hu, R. Ricken, V. Quiring, C. Vannahme, H. Herrmann, D. Büchter, S. Reza, W. Grundkötter, S. Orlov, H. Suche, R. Nouroozi, and Y. Min, "Integrated optical devices in lithium niobate," Opt. Photonics News **19**(1), 24–31 (2008).
16. O. Alibart, V. D'Auria, M. D. Micheli, F. Doutre, F. Kaiser, L. Labonté, T. Lunghi, É. Picholle, and S. Tanzilli, "Quantum photonics at telecom wavelengths based on lithium niobate waveguides," J. Opt. **18**(10), 104001 (2016).

17. S. Bogdanov, M. Y. Shalaginov, A. Boltasseva, and V. M. Shalaev, "Material platforms for integrated quantum photonics," Opt. Mater. Express **7**(1), 111–132 (2017).
18. L. Arizmendi, "Photonic applications of lithium niobate crystals," Phys. Stat. Sol. A. **201**(2), 253–283 (2004).
19. J. J. G. M. van der Tol and J. H. Laarhuis, "A polarization splitter on $LiNbO_3$ using only titanium diffusion," J. Lightwave Technol. **9**(7), 879–886 (1991).
20. N. Goto and G. L. Yip, "A TE-TM mode splitter in $LiNbO_3$ by proton exchange and Ti diffusion," J. Lightwave Technol. **7**(10), 1567–1574 (1989).
21. W. H. Hsu, K. C. Lin, J. Y. Li, Y. S. Wu, and W. S. Wang, "Polarization splitter with variable TE-TM mode converter using Zn and Ni codiffused $LiNbO_3$ waveguides," IEEE J. Sel. Top. Quantum Electron. **11**(1), 271–277 (2005).
22. K. Habara, "$LiNbO_3$ directional-coupler polarisation splitter," Electron. Lett. **23**(12), 614–616 (1987).
23. H. P. Chung, K. H. Huang, S. L. Yang, W. K. Chang, C. W. Wu, F. Setzpfandt, T. Pertsch, D. N. Neshev, and Y. H. Chen, "Adiabatic light transfer in titanium diffused lithium niobate waveguides," Opt. Express **23**(24), 30641–30650 (2015).
24. K. Bergmann, H. Theuer, and B. W. Shore, "Coherent population transfer among quantum states of atoms and molecules," Rev. Mod. Phys. **70**(3), 1003–1025 (1998).
25. G. D. Valle, M. Ornigotti, T. T. Fernandez, P. Laporta, S. Longhi, A. Coppa, and V. Foglietti, "Adiabatic light transfer via dressed states in optical waveguide arrays," Appl. Phys. Lett. **92**(1), 011106 (2008).
26. S. Longhi, "Adiabatic passage of light in coupled optical waveguides," Phys. Rev. E Stat. Nonlin. Soft Matter Phys. **73**(2 Pt 2), 026607 (2006).
27. H. P. Chung, K. H. Huang, K. Wang, S. L. Yang, S. Y. Yang, C. I. Sung, A. S. Solntsev, A. A. Sukhorukov, D. N. Neshev, and Y. H. Chen, "Asymmetric adiabatic couplers for fully-integrated broadband quantum-polarization state preparation," Sci. Rep. **7**(1), 16841 (2017).
28. H. Jin, F. M. Liu, P. Xu, J. L. Xia, M. L. Zhong, Y. Yuan, J. W. Zhou, Y. X. Gong, W. Wang, and S. N. Zhu, "On-chip generation and manipulation of entangled photons based on reconfigurable lithium-niobate waveguide circuits," Phys. Rev. Lett. **113**(10), 103601 (2014).
29. J. Van Roey, J. van der Donk, and P. E. Lagasse, "Beam-propagation method: analysis and assessment," J. Opt. Soc. Am. **71**(7), 803–810 (1981).
30. M. Bazzan and C. Sada, "Optical waveguides in lithium niobate: Recent developments and applications," Appl. Phys. Rev. **2**(4), 040603 (2015).
31. N. V. Vitanov, B. W. Shore, and K. Bergmann, "Adiabatic population transfer in multistate chains via dressed intermediate states," Eur. Phys. J. D **4**(1), 15–29 (1998).
32. S. Y. Tseng, R. D. Wen, Y. F. Chiu, and X. Chen, "Short and robust directional couplers designed by shortcuts to adiabaticity," Opt. Express **22**(16), 18849–18859 (2014).
33. G. Fujii, N. Namekata, M. Motoya, S. Kurimura, and S. Inoue, "Bright narrowband source of photon pairs at optical telecommunication wavelengths using a type-II periodically poled lithium niobate waveguide," Opt. Express **15**(20), 12769–12776 (2007).
34. A. Martin, A. Issautier, H. Herrmann, W. Sohler, D. B. Ostrowsky, O. Alibart, and S. Tanzilli, "A polarization entangled photon-pair source based on a type-II PPLN waveguide emitting at a telecom wavelength," New J. Phys. **12**(10), 103005 (2010).
35. C. W. Wu, A. S. Solntsev, D. N. Neshev, and A. A. Sukhorukov, "Photon pair generation and pump filtering in nonlinear adiabatic waveguiding structures," Opt. Lett. **39**(4), 953–956 (2014).
36. C. Y. Huang, C. H. Lin, Y. H. Chen, and Y. C. Huang, "Electro-optic Ti:PPLN waveguide as efficient optical wavelength filter and polarization mode converter," Opt. Express **15**(5), 2548–2554 (2007).
37. K. S. Chiang, "Construction of refractive-index profiles of planar dielectric waveguides from the distribution of effective indexes," J. Lightwave Technol. **3**(2), 385–391 (1985).
38. C. K. Hong, Z. Y. Ou, and L. Mandel, "Measurement of subpicosecond time intervals between two photons by interference," Phys. Rev. Lett. **59**(18), 2044–2046 (1987).
39. C. H. Lin, Y. H. Chen, S. W. Lin, C. L. Chang, Y. C. Huang, and J. Y. Chang, "Electro-optic narrowband multi-wavelength filter in aperiodically poled lithium niobate," Opt. Express **15**(15), 9859–9866 (2007).
40. W. Ueno, F. Kaneda, H. Suzuki, S. Nagano, A. Syouji, R. Shimizu, K. Suizu, and K. Edamatsu, "Entangled photon generation in two-period quasi-phase-matched parametric down-conversion," Opt. Express **20**(5), 5508–5517 (2012).
41. J. G. Titchener, M. Gräfe, R. Heilmann, A. S. Solntsev, A. Szameit, and A. A. Sukhorukov, "Scalable on-chip quantum state tomography," Quantum Inf. **4**, 19 (2018).
42. K. Wang, J. G. Titchener, S. S. Kruk, L. Xu, H. P. Chung, M. Parry, I. I. Kravchenko, Y. H. Chen, A. S. Solntsev, Y. S. Kivshar, D. N. Neshev, and A. A. Sukhorukov, "Quantum metasurface for multiphoton interference and state reconstruction," Science **361**(6407), 1104–1108 (2018).
43. T. Kroh, A. Ahlrichs, B. Sprenger, and O. Benson, "Heralded wave packet manipulation and storage of a frequency converted pair photon at telecom wavelength," Quantum Sci. Technol. **2**(3), 034007 (2017).
44. K. Wang, S. V. Suchkov, J. G. Titchener, A. Szameit, and A. A. Sukhorukov, "In-line detection and reconstruction of multi-photon quantum states," arXiv:1808.05038.
45. Y. Cao, Y. H. Li, W. J. Zou, Z. P. Li, Q. Shen, S. K. Liao, J. G. Ren, J. Yin, Y. A. Chen, C. Z. Peng, and J. W. Pan, "Bell test over extremely high-loss channels: towards distributing entangled photon pairs between earth and the moon," Phys. Rev. Lett. **120**(14), 140405 (2018).

46. A. Zeilinger, “Light for the quantum. Entangled photons and their applications: a very personal perspective,” Phys. Scr. **92**(7), 072501 (2017).
47. A. S. Solntsev, T. Liu, A. Boes, T. G. Nguyen, C. W. Wu, F. Setzpfandt, A. Mitchell, D. N. Neshev, and A. A. Sukhorukov, “Towards on-chip photon-pair bell tests: Spatial pump filtering in a $LiNbO_3$ adiabatic coupler,” Appl. Phys. Lett. **111**(26), 261108 (2017).
48. A. Boes, B. Corcoran, L. Chang, J. Bowers, and A. Mitchell, “Status and potential of lithium niobate on insulator (LNOI) for photonic integrated circuits,” Laser Photonics Rev. **12**(4), 1700256 (2018).
49. R. Menchon-Enrich, A. Llobera, V. J. Cadarso, J. Mompart, and V. Ahufinger, “Adiabatic passage of light in CMOS-compatible silicon oxide integrated rib waveguides,” IEEE Photonics Technol. Lett. **24**(7), 536–538 (2012).